Translation elongation rate varies among organs and decreases with age

Maxim V. Gerashchenko [ORCID], Zalan Peterfi, Sun Hee Yim [ORCID] and Vadim N. Gladyshev [ORCID]*

Division of Genetics, Department of Medicine, Brigham and Women's Hospital, Harvard Medical School, Boston, MA, USA

ABSTRACT

There has been a surge of interest towards targeting protein synthesis to treat diseases and extend lifespan. Despite the progress, few options are available to assess translation in live animals, as their complexity limits the repertoire of experimental tools to monitor and manipulate processes within organs and individual cells. It this study, we developed a labeling-free method for measuring organ- and cell-type-specific translation elongation rates *in vivo*. It is based on time-resolved delivery of translation initiation and elongation inhibitors in live animals followed by ribosome profiling. It also reports translation initiation sites in an organ-specific manner. Using this method, we found that the elongation rates differ more than 50% among mouse organs and determined them to be 6.8, 5.0 and 4.3 amino acids per second for liver, kidney, and skeletal muscle, respectively. We further found that the elongation rate is reduced by 20% between young adulthood and midlife. Thus, translation, a major metabolic process in cells, is tightly regulated at the level of elongation of nascent polypeptide chains.

INTRODUCTION

Protein synthesis can be classified into three phases - initiation, elongation, and termination, and each phase has been extensively studied. However, most details on intricate mechanisms of translation come from the studies performed in unicellular organisms or *in vitro* cell cultures. While these studies greatly advanced our understanding of molecular mechanisms of protein synthesis, the variability of translation across complex animals is much less understood. Some congenital disorders affecting humans were shown to be caused by dysfunctional translation machinery, e.g. Blackfan–Diamond anemia (1,2). In other instances, potential treatments for disorders such as cystic fibrosis and fragile X syndrome, were designed to intentionally decrease accuracy or the rate of protein synthesis (3). Slowing ribo-

some translocation along the mRNA could partially restore folding of the mutant cystic fibrosis transmembrane conductance regulator protein *in vitro* as well as in a mouse model (3). Therefore, it is important to be able to monitor and manipulate translation in real-time, preferably with the single codon resolution in specific transcripts or even all transcripts at once.

Modern *in vitro* methods allow unsurpassed precision and flexibility, e.g. real-time translation dynamics of a single molecule can be monitored with fluorescent microscopy (4,5), and transcriptome-wide snapshots of translation with a single nucleotide resolution can be achieved by means of ribosome profiling (6–9). In contrast to research performed in cells, few options are currently available to investigate translation in live animals. It is particularly challenging to assess specific steps of translation, i.e. elongation, initiation, or termination rate, *in vivo*. Several approaches were designed, such as feeding animals with amino acid supplements labeled with a stable isotope (10) or radioactively labeled amino acids (11,12); however, none of these methods are easily scalable and often require months to set up an experiment.

We were guided by these challenges and the need to assay various steps of translation in various organs of live animals at an individual gene level. In this work, we developed a technique to directly assess translation *in vivo* and measure organ- and cell-specific translation elongation rates and other features of protein synthesis. Our method requires no radioactive labeling nor transgenic reporters and can be applied to a variety of small animals such as a mouse or a rat. It relies on two translation inhibitors injected directly into the bloodstream in a time-dependent fashion. The first inhibitor (harringtonine) blocks initiation of translation without affecting elongation. The second inhibitor (cycloheximide) is injected after a specified time (less than a minute) to block elongation. Thus, the time-dependent runoff of ribosomes is detected after the analysis of sequencing data and the elongation rate and other features of translation are inferred. Previous studies demonstrated this principle to work in cell culture (7), whereas we implemented it *in vivo*. We measured elongation rates in three mouse organs and showed that they differ by >50% in the rate. We

*To whom correspondence should be addressed. Tel: +1 617 525 5122; Email: vgladyshev@rics.bwh.harvard.edu

further applied this method to investigate how translation elongation changes with age. While some studies suggested that translation declines with age, since there are many factors influencing protein yield (initiation rate in particular), it has not been clear whether the elongation rate decreases as well or stays constant. By measuring the translation elongation rate in the livers of young and old mice, we directly demonstrated the decline in the elongation rate with age.

MATERIALS AND METHODS

Translation inhibitors used in experiments

Lactimidomycin was purchased from EMD Millipore. Harringtonine was available from three vendors: Abcam, Santa Cruz Biotechnology, and Carbosynth. We tested all three sources and found no difference in quality and toxicity. Most of the experimental work was done with the chemical supplied by Abcam. Cycloheximide was purchased from Sigma-Aldrich.

Drug delivery in mice

We used two injection routes: a tail vein and a retro-orbital sinus. Retro-orbital injection requires little practice and is convenient for single drug delivery (13). It is quite invasive, therefore, we sedated mice with the intraperitoneal injection of pentobarbital (20 mg/kg). Tail veins are more appropriate for accurately timed double injections. There are two large lateral veins in the mouse tail. We attached catheters to both veins and connected them to syringes filled with harringtonine or cycloheximide. During the entire procedure, mice were sedated with a continuous flow of 1% isoflurane mixed with oxygen (Visualsonics, Vevo anesthesia system) and kept on a heated pad. Sedation caused no significant change in translation based on analyses of polysomes on the sucrose gradient. In a typical experiment, we injected 200 ul of harringtonine (5 mg/ml) in phosphate buffer saline (PBS), followed by 100 ul of cycloheximide (20 mg/ml) in the same buffer. Cycloheximide is highly soluble in the buffer. Harringtonine, on the other hand, is poorly soluble in aqueous solutions; therefore, 50 mg/ml stock was prepared in dimethyl sulfoxide and 20-fold dilution in phosphate buffer saline was made fresh right before the injection. Lactimidomycin was prepared similarly. The highest dose of lactimidomycin that we could administer was 200 ul of a 0.25 mg/ml solution in 20% dimethyl sulfoxide, 80% PBS. Several attempts were made to increase the amount of harringtonine cycloheximide that could be delivered to a mouse. Supplementing PBS with 40% (2-hydroxypropyl)-β-cyclodextrin (Sigma) increased cycloheximide solubility up to 60 mg/ml without any toxic response from mice. It did not help with harringtonine or lactimidomycin solubility. Heart function was monitored by ECG (AD Instruments, Powerlab 8/30 recorder with BioAmp electrodes). Animals with a severe drop of heartbeat or incomplete injection were excluded from the analysis. Control mice (0 sec timepoint) were injected with blank PBS.

Animals

All mice used in this study were C57BL/6J males. Younger mice were 3 months of age (Jackson Lab) and older mice 18 months (NIA aged rodents program). Experimental animal protocols were approved by the Institutional Animal Care and Use Committee at the Brigham and Women's Hospital, Harvard Medical School.

Harvesting tissues

Unless otherwise stated, in the case of a single inhibitor injection, we held a mouse asleep for 5 min before euthanizing it by cervical dislocation. Mice with time-course injections of two inhibitors were prepared for ~3 min (sedating with isoflurane, connecting electrodes and the tail vein catheter), proceeded with injections for the specified duration, and kept alive for 1 min after the second inhibitor injection, then euthanized by the cervical dislocation. Nine organs were collected, always in the same order (liver, lungs, heart, kidney, spleen, pancreas skeletal muscle—lower limbs, testes and brain). Large organs were cut in slices, snap-frozen in liquid nitrogen, and stored at −80 °C. Organ harvesting took no more than 3 minutes after the cervical dislocation.

Ribosome profiling

In a typical experiment, we used 30 mg of the liver, 60 mg of a kidney and 200 mg of skeletal muscle to extract ribosomes. Soft tissues, such as the liver, kidney, pancreas, and brain were lysed in a glass-Teflon Dounce homogenizer filled with the ice-cold buffer. Tough tissues, such as heart, skeletal muscles, and lungs were first pulverized in a ceramic mortar-pestle filled with liquid nitrogen, then lysed a glass-Teflon Dounce homogenizer. Based on our previous experience, RNase S7 and T1 are the best ribonucleases for ribosome footprint generation in mouse organ lysates (9). Lysates from control, non-injected, and harringtonine-injected mice were treated with the 4:1 mixture of RNase T1 (Epicentre, cat# NT09500K) and RNase S7 (Roche/Sigma, cat# 10107921001). RNase S7 comes as powder and the 10 mg/ml stock was made in 10 mM Tris–HCl pH 7.5, 50 mM NaCl, 1 mM EDTA, 50% glycerol. Tissue lysates from mice used in time-course experiments were treated with RNase T1 alone. Different organs required specific lysis conditions. Lysis buffer composition for liver and kidney was as follows: 20 mM Tris–HCl pH 7.5, 100 mM KCl, 5 mM $MgCl_2$, 1 mM DTT, 1% Triton, 0.1 mg/ml cycloheximide. Lysis buffer composition for skeletal muscle: 20 mM Tris–HCl pH 7.5, 100 mM KCl, 5 mM $MgCl_2$, 1 mM DTT, 1% Tween-20, 0.25% Deoxycholate, 0.1 mg/ml cycloheximide. Lysis buffer composition for lung, pancreas, spleen, heart, brain and testis: 20 mM Tris–HCl pH 7.5, 100 mM KCl, 5 mM $MgCl_2$, 1 mM DTT, 1% Tween-20, 0.25% Deoxycholate, 0.1 mg/ml cycloheximide. For preparative purposes, i.e. when ribosomes were used for footprint extraction and sequencing, we kept 5 mM $MgCl_2$ in lysis buffers. For quality checks and sucrose gradient analyses, we increased $MgCl_2$ up to 10 mM. Lysis buffers were also supplemented with protease inhibitors (Roche) and 5 mM $CaCl_2$ as RNase S7 was applied. Sucrose gradients were always 10–50% sucrose in 20 mM Tris–HCl pH 7.5, 100 mM KCl, 10 mM $MgCl_2$, 1 mM DTT, 0.1 mg/ml cycloheximide. Fractionation was performed by ultracentrifugation for 3 h at 35 000 rpm in an SW41 rotor (Beckman, Optima L-20K) at 4°C. After the centrifu-

gation, gradients were passed through a UV detector (Bio-Rad) and the absorption at 254 nm was recorded. The fraction containing monosomes was collected in a single tube if necessary. The volume of the sample was brought to 50 ul by concentrating it using 100 kDa filters (Amicon Ultra, Millipore). Then, the sample was diluted to 500 ul with a buffer containing 10 mM Tris–HCl pH 7.5, 2 mM EDTA, 1% SDS. RNA was extracted by hot acid phenol (Ambion) and precipitated by the glycogen-ethanol method (1/10 volume of 3 M sodium acetate, 1/100 volume of glycogen, 2.5 volumes of pure ethanol, 1-hour incubation at −20 °C followed by centrifugation). RNA was loaded on a 15% polyacrylamide TBE-urea gel and the band containing ribosomal footprints around 28 nucleotides was cut. Subsequent steps were the same as described in (9).

Transcriptome library preparation

Total RNA was extracted from tissues with Trizol (Ambion) and purified using Direct-zol 96-well plate RNA kit (Zymo Research). The sample quality was checked with TapeStation (Agilent). Every tissue except the pancreas had the RNA integrity number (RIN) higher than 8.7 which indicates high-quality RNA. Extraction of intact RNA from the pancreas is hardly possible due to the presence of the endogenous RNase A in high amounts, therefore we proceeded with sequencing although the RIN was ∼6.

High throughput sequencing and data processing

Ribosome profiling libraries were sequenced on the Illumina HiSeq 2000 and NextSeq 500 platforms at the Harvard University Bauer Core. mRNA-seq libraries were sequenced on the Illumina HiSeq 4000 in the paired-end mode at the Novogene Inc. Adapters were removed from ribosome profiling reads with Cutadapt software (cutadapt -u 1 -m 23 -a AGATCGGAAGAGCACACGTCT) (14). mRNA-seq sequences were aligned with TopHat 2.1.0 using following settings: tophat –transcriptome-index –no-discordant –no-mixed –no-novel-juncs (15).

The NCBI mouse genome build GRCm38.p3 and the *Mus musculus* Annotation Release 105 were used as a reference. When aligning mRNA-seq and ribosome profiling reads for expression and translation efficiency estimation we used the following strategy. Only full chromosomes were left, and all non-chromosomal and mitochondrial records were removed. Furthermore, only RefSeq and BestRefSeq records were left in the transcriptome annotation, while Gnomon predictions were discarded along with pseudogenes. Read count per gene was accessed by HTseq-count software (16).

To plot time-dependent ribosome occupancy, we employed a different strategy. First, using a gene bank (gbk) file, which comes in a package with the genome assembly and annotation, we extracted RefSeq and BestRefSeq records for every gene including CDS, 5′-UTR and 3′-UTR lengths and sequences. Among them, we identified the longest isoform for every gene, prioritized as CDS > 5′UTR > 3′UTR. 5′-UTRs were trimmed by 100 nucleotides. If either of the annotated UTRs was shorter than 100 nucleotides, we extended it based on genomic coordinates. To prepare a list of non-redundant genes, we run *blast* of all vs. all (blastall -p blastn -m 8 -b 500 -v 500 -e 0.001). Gene pairs that are too similar at the level of nucleotide sequence were excluded. In addition to the e-score, we enforced a requirement of the high-homology stretch being at least 50 nt long, and if it was longer, the similarity had to be at least 90% to treat these genes as homologous and redundant. A total of 13 685 genes passed every threshold. This reference set ensured the unambiguous alignment of ribosome footprints.

Calculating translation elongation rate

Since a single mouse was an independent timepoint, we employed a simple linear model *distance ∼ time*. The distance is defined as the number of codons from the initiation start site to the point on the normalized read density curve where it equals half of its maximum value. The maximum value for any given curve is averaged over 500 nucleotides where it reaches a plateau (positions 1000–1500 from the initiation start site).

Gene set enrichment analysis

To identify pathways associated with genes with significantly high or low translation efficiency across tissues, we used *limma* software (17) to calculate the *P*-value for each gene against the null hypothesis that the average translation efficiency of the gene is equal to the average translation efficiency across the whole transcriptome. When several replicates of the same tissue were present, we considered the translation efficiency of every gene for the corresponding tissue as an average across all replicates. Then we performed a pathway GSEA on a pre-ranked list of genes (18). For every gene, this list contained z-score, calculated as:

$$-ln(P)*S,$$

where *P* is the *P*-value calculated as described previously and *S* is the sign of the difference between the average TE of the gene and average TE across the whole transcriptome. Kyoto Encyclopedia of Genes and Genomes (KEGG), Reactome, Biocarta, Gene Ontology (GO) Biological Process (BP) and Molecular Function (MF) databases were used in this analysis.

Cluster analysis

Translation efficiency (TE) for individual genes was calculated as Ribo-seq read counts divided by mRNA-seq counts. Only genes expressed in all organs were taken into the analysis (≥ 10 reads in every organ and sequencing type, 4782 genes satisfied these criteria). Normalization across organs was performed by centering TE values distribution at 0 and dividing by the standard deviation. Organs were hierarchically clustered by a complete linkage method using the Pearson correlation distance (1 − cor). Genes were hierarchically clustered by the Ward method using the Euclidean

distance. The genes dendrogram was further sorted by *dendsort* R package with default settings (19).

RESULTS

Translation inhibitors perform well in live mice

Translation inhibitors typically have a well-defined mechanism of action, and some inhibitors are specific to particular phases of translation. We selected two translation initiation inhibitors known to selectively target translation initiation: lactimidomycin (20) and harringtonine (21). Both inhibitors work *in vitro* when added to the cell culture medium (7). To test whether these inhibitors affect translation upon injection in the mouse bloodstream, we performed retroorbital injection (13) to a cohort of 3-month-old C57BL/6 male mice (Figure 1A). These inhibitors are expected to cause depletion of the polysomal fraction, which can be assessed by sucrose gradient fractionation of organ lysates. Out of two inhibitors, only harringtonine reliably depleted polysomes in a wide range of concentrations. It is also much more affordable compared to lactimidomycin, an important factor considering the amounts needed per mouse.

Within 5 min, harringtonine (0.5–4 mg/mouse) completely depleted polysomes in all organs except for testes and brain, where up to 30 min were needed to significantly reduce the number of polysomes due to the blood-brain and blood-testis barriers (Figure 1B, Supplementary Figure S1). Harringtonine specificity was further confirmed by sequencing mRNA fragments trapped within the ribosome active core, the method also known as ribosome profiling or Ribo-seq. Post-treatment ribosomes were almost exclusively located near the start codons, agreeing with the notion that harringtonine primarily affects the initiation of translation (Figure 1C). During these experiments, we noticed that the high doses of harringtonine may cause cardiac arrest in some animals; therefore, we adjusted the dosage and monitored the heart function with the electrocardiogram (ECG, Figure 2A). The optimal dose was found to be 200 ul of harringtonine (2.5 mg/ml) in the phosphate buffer saline per 20–25 g animal (Figure 2B). Next, we co-injected harringtonine with varying doses of cycloheximide (20–60 mg/ml) to test the efficacy of the latter. When administered together, these drugs should not have a noticeable effect on the polysome profile, which is exactly what we observed (Supplementary Figure S2A). Hence, both inhibitors were active *in vivo* and had comparable uptake rates across tissues.

We also followed on the reports suggesting that translation can be affected by volatile anesthetics such as halothane and isoflurane (22,23). In these studies, organs were perfused *in situ* with a high concentration of the anesthetic for an extended duration of time (>15 min). These conditions are rather extreme compared to our experimental setting: we delivered isoflurane via inhalation at a much lower concentration and the entire exposure to the anesthetic did not last for more than 5 min. Nevertheless, no effect of isoflurane on translation was observed under our experimental conditions, which further validated the protocol (Supplementary Figure S2B).

Two translation inhibitors can be used to produce a time-dependent shift in ribosome occupancy

Given the two translation inhibitors performing well in live mice, we set up a pulse-chase experiment with the harringtonine injection followed by cycloheximide injection. Since it is difficult to do two injections retro-orbitally within a narrow timeframe, we delivered inhibitors through the tail vein. The setup included two catheters connected to syringes filled with translation inhibitors and inserted to each of the two major lateral tail veins (Figure 2C). The experiment was initiated by the injection of harringtonine and followed by the injection of cycloheximide after a specified time (Figure 3A-B). The heart was still functioning normally during and after injections, pumping the blood and fully supporting organ functions. Mice were euthanized by cervical dislocation 1 min after the injection of cycloheximide. Prior to selecting samples for sequencing, we tested different intervals between harringtonine and cycloheximide injections, ranging from 15 to 120 s on the sucrose gradient, and found that 15, 30 and 45 s time points were optimal (Supplementary Figure S3). To precisely measure the translation elongation rate, we used 3–4 animals per time point, three time points in total. The resulting ribosome profiling libraries from three organs (liver, kidney, and skeletal muscle) were sequenced. Linear regression analysis of ribosome coverage tracks estimates the translation rates of 6.8, 5.0, 4.3 amino acids per second for liver, kidney and skeletal muscle, respectively (Figure 3C, D, Supplementary Figure S4). Figure 3E shows the cumulative ribosome coverage of open reading frames in these samples. Time-dependent run-off is evident in every organ, and, interestingly, the rate was different between the organs which may reflect the metabolic load. These rates can be compared to that previously estimated in mammalian cell culture (5.5 aa/s) by Ribo-seq (7,24) and in rat liver (∼5.7 aa/s) by radioactive labeling (11,25).

It is not entirely clear how fast the injected inhibitors were delivered by the bloodstream to the organs. There was an upper estimate of 5 min obtained from the retroorbital injections, but the lower bound is unknown. In a previous experiment performed with a mouse cell line, there was an ∼90 s delay after adding harringtonine and before harringtonine showing the effect on translation (7). In our experimental setup, we tightly controlled the interval between injections. Many unknown variables may affect inhibitors' uptake, such as the blood flow rate and the rate of passive diffusion from capillaries to cells in different organs. The organ-specific properties of inhibitors' delivery should stay constant across time points, which means that the only important parameter is the time period between the harringtonine and cycloheximide injections. Because of that, the control time point (0 s) was not used in calculations. As a result, we were able to capture and quantify the ribosomal run-off within as little as 15 s in live mice (Figure 3C–E), and even narrower time intervals are possible.

Selecting proper time points and the injection route is critical to accurately measure the translation elongation rate

As discussed above, the original 5 min long incubations with harringtonine resulted in sharp peaks at the translation start sites. However, ribosomes were still very abun-
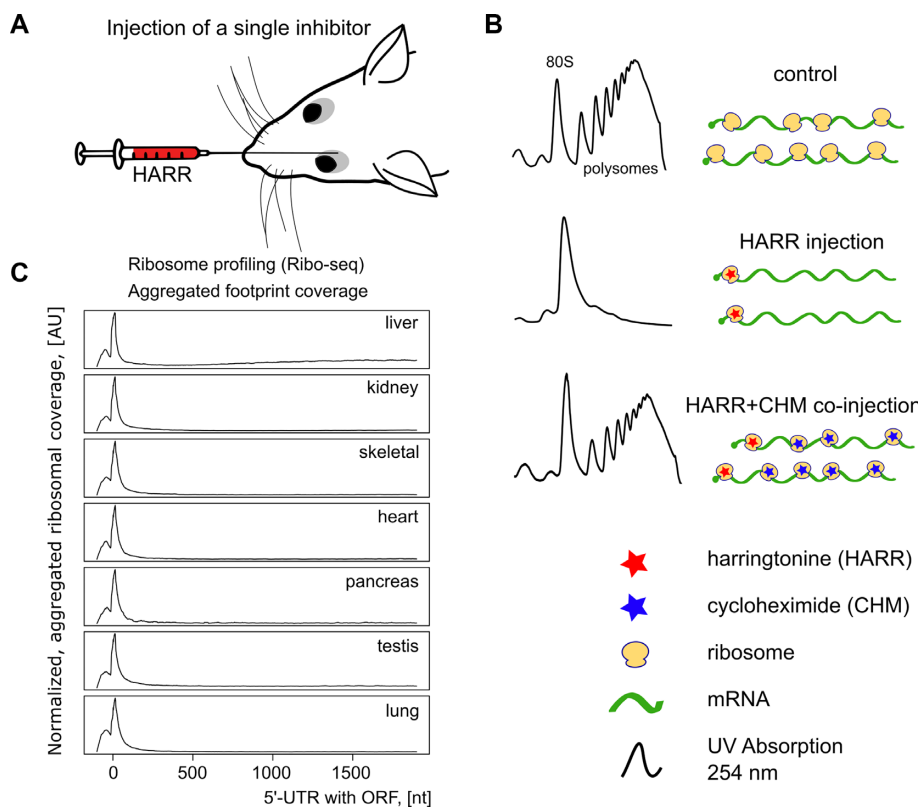
Figure 1. Evaluating translation inhibitors *in vivo*. (**A**) Single injection done to retroorbital cavity around the eye. (**B**) Both translation inhibitors show similar efficiencies and uptake times following injection into the bloodstream. Using sucrose gradient profiles of the mouse liver as an example, we demonstrate that harringtonine depletes polysomes while co-injection with cycloheximide preserves polysomes. (**C**) Harringtonine performance in 7 organs. It effectively stalls ribosomes at the vicinity of start codons. Post-injection incubation time was 5 min except testes, where up to 30 min were required to pass the blood-tissue barriers. Zero corresponds to the start of the open reading frame. 100 nucleotides from the 5′-UTR were added to allow mapping footprints over the start codon.

dant at the distant downstream regions of mRNAs in the liver as can be seen at the metagene level (Figure 1C) as well as in individual gene cases (Figure 4). This effect appeared exclusively in the liver and, at first, we hypothesized that it may be due to the lower blood pressure in the retroorbital sinus and thus less efficient spread of translation inhibitors by the vascular system. However, a similar outcome was observed when injections were performed through the tail vein. Perhaps, the cellular concentration of harringtonine could reach the level inhibitory to elongation, because we administered much more drug compared to the *in vitro* study (7). It could also explain why the liver is the most affected organ in our set. Unlike the heart and skeletal muscle, the liver has sinusoidal (discontinuous) capillaries with large gaps in the basal membrane and between epithelial cells (26). It facilitates the exchange of larger biomolecules between blood and hepatocytes and increases the diffusion rate in general. Therefore, if harringtonine can interfere with elongation at high cytoplasmic concentrations, it should affect the liver in the first place. On a related note, given more timepoints and better time resolution, we encountered a sudden drop in the observable translation elongation rate past 45 sec not only in the liver but in other organs too. When the samples corresponding to 60 s time points were sequenced and analyzed for the liver, kidney, and skeletal muscle, a decline in the observed translation rate was observed compared to the 15–45 s interval (Sup-

plementary Figure S5). No retardation of the translation elongation rate was previously observed in a study involving mouse cell culture, where the first timepoint was at 90 s (7). Similarly, no translation shutdown was reported when radioactive amino acids were used to estimate the elongation rate in rats and toadfish livers (11,12,25). Investigation of the mechanism involved is a goal of our future studies.

In addition to the translation elongation rate, we could assess translation initiation *in vivo*, without prior cell extraction and thus without perturbing physiological conditions. In this regard, it provides a viable alternative to current approaches (27–31). It must be noted that translation inhibitors inadvertently introduce biases in the start codon selection, especially upstream of conventional open reading frames (8). The height of ribosome occupancy peaks in ribosome profiling tracks should not be treated as an accurate indicator of the physiological initiation efficacy. Yet, it can be used to highlight potential translation initiation sites. Ribosomes accumulate at the translation start sites overtime after the harringtonine injection. This applies both to the classical open reading frames (Figure 4) and regulatory upstream reading frames as can be seen in the case of the *Atf4* transcript - the well-known example of translational regulation mediated by upstream ORFs (Figure 5A). There are tissue-specific patterns of uORF utilization, and *in vivo* experiments can provide new insights into translational regulation of gene expression.
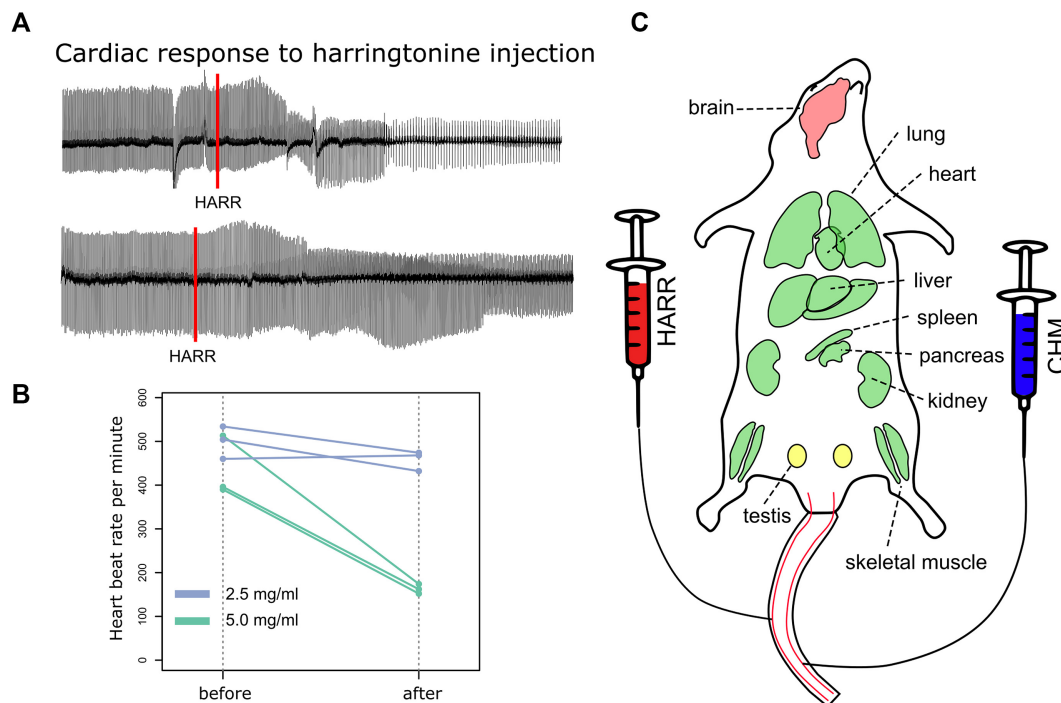
Figure 2. Experimental setup for double injections. (**A**) Representative electrocardiograms (ECG) from injected mice. The upper track shows the slowdown of the beat rate in response to 5 mg/ml harringtonine. The lower track shows no difference after the injection of 2.5 mg/ml harringtonine. The effect of harringtonine appears roughly 20 s after the injection. The red line marks the injection event. (**B**) High doses of harringtonine severely drop heartbeat rate. We established that 2.5 mg/ml had no effect on the beat rate, whereas 5 mg/ml decreased it twice. 10 mg/ml caused cardiac arrest in most cases. All injections were done via the tail vein − injection volume was 200 ul and the weight of mice was 20–25 g. (**C**) The layout of mouse organs susceptible to translation inhibitors. Organs marked in green are permeable for both harringtonine and cycloheximide within 15 s post-injection. Translation elongation rate can be directly measured in these organs. Testes (shown in yellow) are partially permeable, and brain is mostly unaffected by inhibitors.

Alternatives to tail vein injections

Tail vein delivery of inhibitors is convenient when multiple organs are harvested. It is less convenient if one is only interested in measuring translation rates in a single organ. In either case, the number of mice is the same and a single mouse represents a single time point. We attempted to reduce the number of mice by performing an *ex vivo* liver perfusion followed by slicing off liver pieces and freezing them in liquid nitrogen, thus generating a series of time points from a single animal. Mouse liver was separated from the rest of the vascular system and a phosphate buffer saline or physiological saline containing harringtonine was pumped through. Unexpectedly, no effect on polysomes was observed (Supplementary Figure S6A). The lack of translation inhibition was reproducible at various perfusion rates and inhibitor concentrations. At the same time, directly injecting harringtonine to the tail vein, portal vein (entry to the liver), femur vein, and retro-orbitally always resulted in robust polysome depletion. We conclude that the vascular system should maintain its integrity throughout the entire duration of the experiment. This finding was further strengthened by the fact that even with the direct drug injection to the portal vein, the moment we cut off the first liver piece and compromised vascular integrity, any subsequent piece had a very slow polysome depletion rate (Supplementary Figure S6B).

Measuring translation efficiency across multiple organs

We further complemented ribosome profiles with transcriptomes from the same organs. The ratio of Ribo-seq to mRNA-seq counts is often used to estimate translation efficiency (TE). It reflects how well the transcript is translated compared to other transcripts from the same organ. Transcripts with higher translation efficiency yield more protein molecules given the same number of transcripts. Calculating this ratio for every single transcript gives us the list of organ-specific translation efficiencies for thousands of proteins. TE values across different organs display a high degree of variance. Transcripts with high TE in one organ have low TE in another organ. It is hard to find a group of genes in which TE values would be the same across all organs (Supplementary Figure S7). Overall, the liver and kidney are the closest to each other with a good correlation coefficient (Spearman $\varrho = 0.887$, Supplementary Figure S8). Genes with high TE values in the liver are likely to have high TE in the kidney. Other organs have unique TE patterns that set them apart from each other.

Gene set enrichment analysis revealed that pathways involved in metabolism were enriched in genes with higher translation efficiency. These pathways included the TCA cycle, oxidative phosphorylation, fatty acid metabolism, and glycolysis. On the other hand, mTOR signaling, MAP kinase signaling, insulin signaling, and ribosome (as a GO
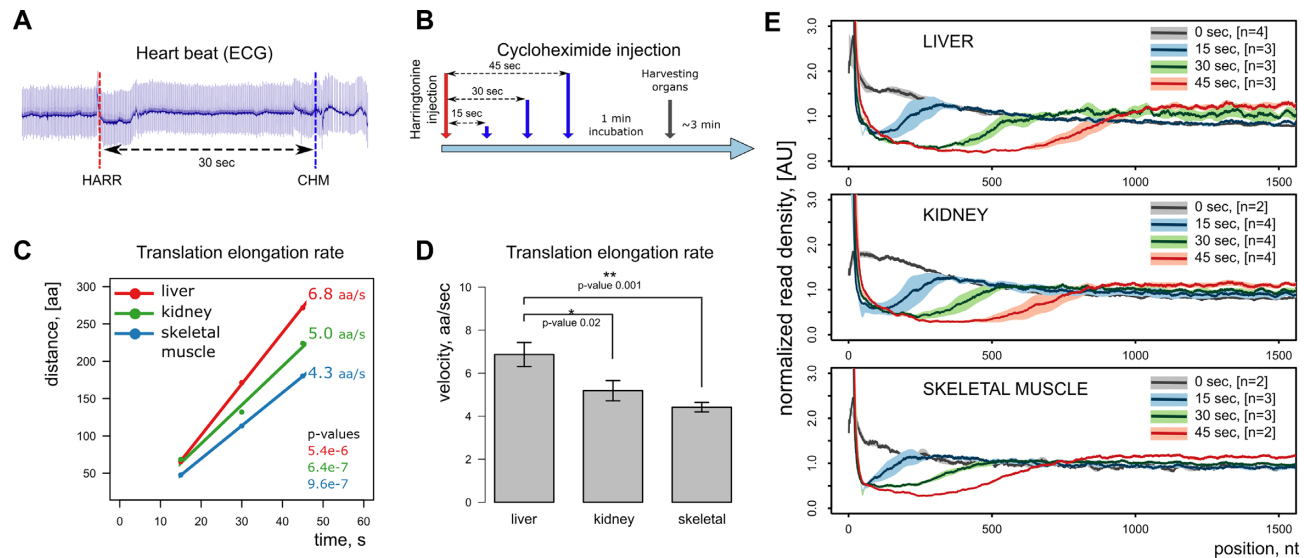
Figure 3. Measuring organ-specific translation elongation rate *in vivo*. (**A**) ECG monitoring of heart function before and after drug injection to ensure the heartbeat rate is unaffected at the chosen dosage. (**B**) Experimental design for a time-resolved study. (**C**) Linear regression analysis of injection timepoints to infer the elongation rate. (**D**) Comparison of mean translation elongation rates in three organs. Statistical significance was accessed with a linear model *distance ∼ time*, error bars represent the standard error and the number of samples is identical to the panel E (excluding controls). (**E**) Metagene analysis of ribosome profiling sequences. Genes longer than 2000 nucleotides are presented (refer to Supplementary Figure S4 for gene length selection). The first 1500 nucleotides are shown starting from the first codon of the reading frame. Solid lines represent mean signal from biological replicates, and light shading corresponds to a standard deviation. 0 s timepoint refers to control animals injected with PBS.
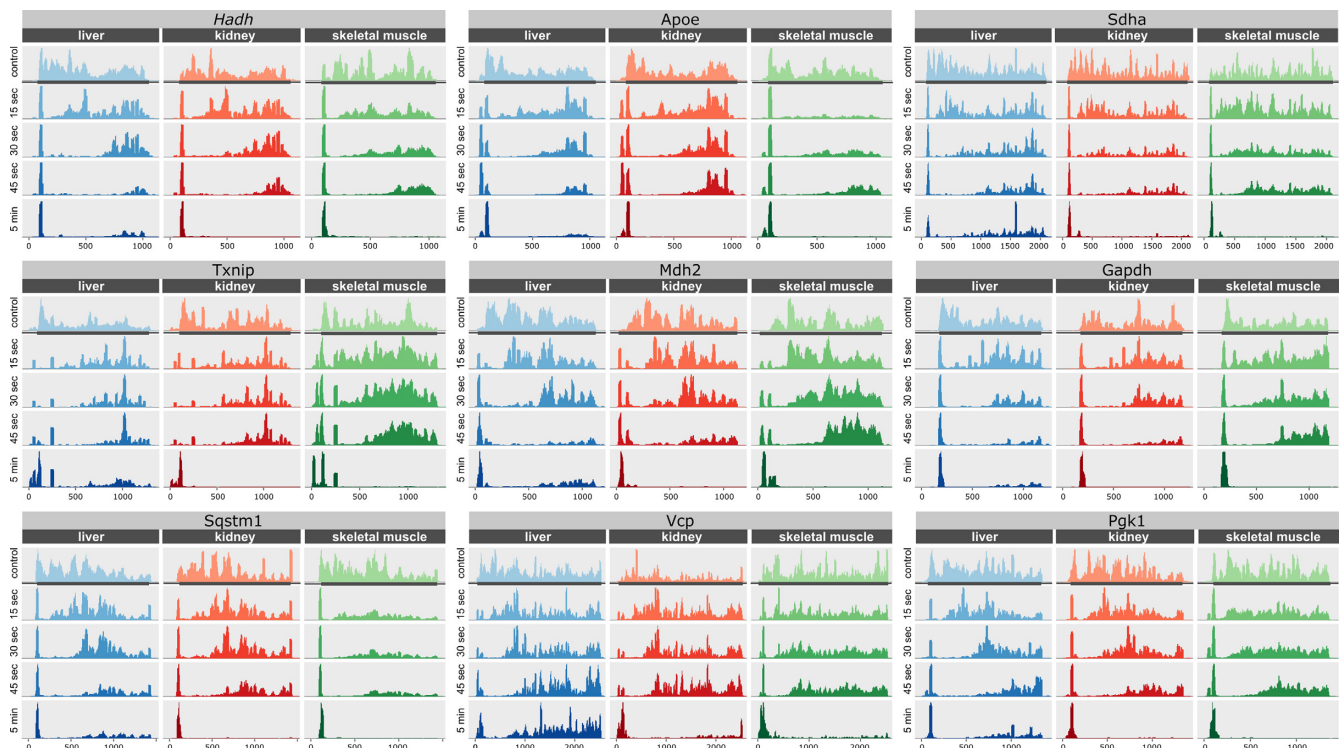

Figure 4. Ribosome footprint profiles of representative transcripts. Transcripts were selected among those highly expressed in three organs: liver, kidney and skeletal muscle. For each transcript, the entire ORF was selected with extra 100 nucleotides from 5′- and 3′-UTRs. The ribosomal run-off is a consequence of the harringtonine injection. The entire ORF with 100 nucleotides from the 5′ and 3′ UTRs is shown. The sharp peak on the left side of each plot corresponds to ribosomes stalled at the translation start site by harringtonine. Annotated ORF is marked with the grey rectangle.
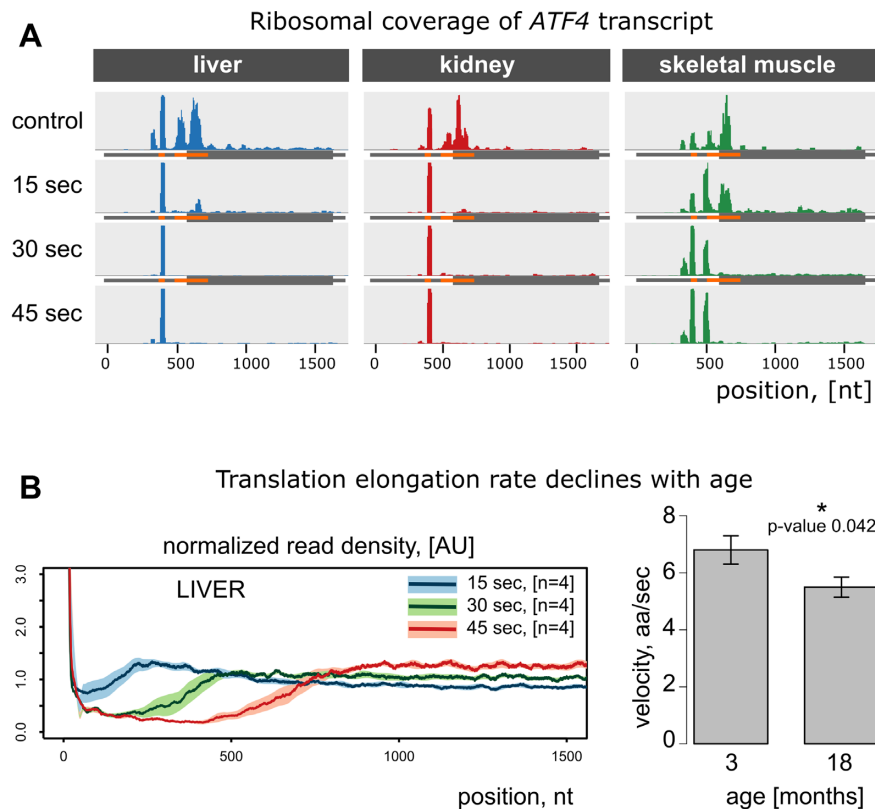
Figure 5. Time- and age-dependent changes in translation. (**A**) Ribosome footprint coverage of ATF4 transcript. This gene is a classic example of post-transcriptional regulation mediated by upstream reading frames (uORFs). It has 2 uORFs, shown in orange. Shortly after the injection of harringtonine, ribosomes are stalled at the start codons of the corresponding uORFs. Interestingly, there are two peaks in skeletal muscle samples: one at the first uORF and another at the second. However, there is only a single peak in liver and kidney. (**B**) The elongation rate declines with age. Left: estimation of translation elongation in liver was done as in Figure 3E, but 18-month-old mice were used. Right: Liver translation between two groups of mice (3- and 18-month-old) was compared. Mean elongation rates (aa/sec) were measured as 6.8 at the young age and 5.5 at the older age.

term) were enriched with genes with lower translation efficiency (Supplementary Figure S7).

Translation elongation rate decreases with age

We applied our new method to young (3-month-old) and older (18-month-old) animals. It is thought that translation, like many other physiological processes, declines with age in different species. However, it is not clear which translation phase is affected as an organism ages. The net translation can be brought down by inefficient initiation, slower elongation, or other factors such as ribosome abundance and mRNA availability. Since our method allows measuring the rate of elongation independent of initiation, we directly measured the elongation rate in the liver of young and old mice. We found that the rate of elongation decreased by ∼ 1.3 aa/sec in old compared to young mice, which represents a nearly 20% decrease (Figure 5B). The rate of elongation in the liver of 18-month-old mice was almost the same as in the kidney of young mice. Given the average mouse lifespan of 30 months, it is reasonable to expect an even larger decline in the elongation rate near the end of life.

DISCUSSION

We found that translation elongation rate varies among organs and decreases with age. To arrive at these conclusions,

we developed and utilized a method to assess translation elongation rates *in vivo*. This method should be widely applicable to rodents and likely other animals.

We explored the feasibility of measuring translation elongation in multiple organs and proved that it is possible even within very narrow time intervals. In the current study, we focused on three representative tissues which were assessed at three timepoints. While this has been sufficient to estimate mean translation rate with high precision, in future experiments gene-specific translation rates will require better temporal resolution. Our method presents new opportunities for animal studies, such as studying the effects of ribosome protein mutations, dietary interventions, or other factors on translation.

Translation elongation rates differed more than 50% among organs, with the highest in the liver, and lowest in the skeletal muscle. This is generally consistent with the metabolic rates of these organs. The rates we quantified were also consistent with previous analyses in ES cells in culture (7,24) as well as with radiolabeling data (11,25). The previous elongation rates 5.2–5.5 amino acids per second were within the range we determined for various tissues (4.3–6.8 amino acids per second).

One concern we had prior to this study is related to the properties of albumin. It contains multiple hydrophobic binding pockets to retain and transport fatty acids, steroids,

and drugs. For example, in a time-course experiment in cell culture, harringtonine was mostly bound by albumin coming from the bovine serum supplement. For this reason, we injected high amounts of harringtonine and cycloheximide into the bloodstream. Although it is hard to estimate the dynamics of translation inhibitors uptake by cells *in vivo*, our results indicate that the minimal effective drug concentration could be lower than that used in this study. It is also possible that a lower amount of harringtonine might not interfere with elongation at later time points (above 45 s).

We also detected a significant decline in the elongation rate with age ($\sim$20%) by analyzing the livers of 3- and 18-month-old mice. Our observations are in line with the consensus that biological processes and their regulation become less robust as the organism ages. Age-related changes in protein synthesis have not yet been studied to the same extent as proteome maintenance and protein degradation. Bulk protein synthesis declines with age (32,33). However, translation is a multi-step process, so the decline could happen at any stage: initiation, elongation, and termination. Some lifespan-extending dietary interventions, such as methionine restriction (34) and rapamycin supplementation (35), are known to impact translation. Separating the input of each of these stages *in vivo* is very challenging. Recently, we showed the age-dependent decrease in the expression of ribosomal proteins and translation initiation factors in the liver and kidney of mice using ribosome profiling (36). Our current study complements previous results and shows that the age-dependent decline in protein synthesis occurs at multiple stages. It would be interesting to access the consequences of slow elongation in future studies. In theory, the slower elongation rate should lower mistranslation (37). On the other hand, it should also affect co-translational protein folding which could have both positive and detrimental consequences.

Concluding, quantitative assessment of translation elongation rate in live organisms offers important reference information on this important metabolic process. The new method we describe allows measuring the elongation rates in various organs and cell types *in vivo*. In addition, the method captures the profiles of the translation start sites, upstream reading frames, and organ-specific translation efficiency. Elongation rates may be influenced by multiple factors, such as post-translational modifications of ribosomal proteins, local levels of amino acids, and tRNA concentrations. The finding of the rapid delivery of translation inhibitors to mouse organs would allow the use of additional effectors, targeting termination and various mechanisms of regulation of protein synthesis. Proteostasis is known to be associated with physiological conditions such as aging (38), cancer (39) and ribosomal pathologies (40), and we directly observed the decreased elongation rate in aging animals.

DATA AVAILABILITY

Raw sequencing data can be accessed through the GEO repository, accession number GSE112223. Bioinformatics pipelines and supplementary code is available here https://github.com/germaximus/ElongationRate.

SUPPLEMENTARY DATA

Supplementary Data are available at NAR Online.

REFERENCES

1. Khajuria,R.K., Munschauer,M., Ulirsch,J.C., Fiorini,C., Ludwig,L.S., McFarland,S.K., Abdulhay,N.J., Specht,H., Keshishian,H., Mani,D.R. *et al.* (2018) Ribosome levels selectively regulate translation and lineage commitment in human hematopoiesis. *Cell*, **173**, 90–103.
2. Mills,E.W. and Green,R. (2017) Ribosomopathies: There's strength in numbers. *Science*, **358**, eaan2755.
3. Oliver,K.E., Rauscher,R., Mijnders,M., Wang,W., Wolpert,M.J., Maya,J., Sabusap,C.M., Kesterson,R.A., Kirk,K.L., Rab,A. *et al.* (2019) Slowing ribosome velocity restores folding and function of mutant CFTR. *J. Clin. Invest.*, **129**, 5236–5253.
4. Morisaki,T., Lyon,K., DeLuca,K.F., DeLuca,J.G., English,B.P., Zhang,Z., Lavis,L.D., Grimm,J.B., Viswanathan,S., Looger,L.L. *et al.* (2016) Real-time quantification of single RNA translation dynamics in living cells. *Science*, **352**, 1425–1429.
5. Yan,X., Hoek,T.A., Vale,R.D. and Tanenbaum,M.E. (2016) Dynamics of translation of single mRNA molecules in vivo. *Cell*, **165**, 976–989.
6. Ingolia,N.T., Ghaemmaghami,S., Newman,J.R. and Weissman,J.S. (2009) Genome-wide analysis in vivo of translation with nucleotide resolution using ribosome profiling. *Science*, **324**, 218–223.
7. Ingolia,N.T., Lareau,L.F. and Weissman,J.S. (2011) Ribosome profiling of mouse embryonic stem cells reveals the complexity and dynamics of mammalian proteomes. *Cell*, **147**, 789–802.
8. Gerashchenko,M.V. and Gladyshev,V.N. (2014) Translation inhibitors cause abnormalities in ribosome profiling experiments. *Nucleic Acids Res.*, **42**, e134.
9. Gerashchenko,M.V. and Gladyshev,V.N. (2017) Ribonuclease selection for ribosome profiling. *Nucleic Acids Res.*, **45**, e6.
10. Claydon,A.J., Thom,M.D., Hurst,J.L. and Beynon,R.J. (2012) Protein turnover: measurement of proteome dynamics by whole animal metabolic labelling with stable isotope labelled amino acids. *Proteomics*, **12**, 1194–1206.
11. Mathews,R.W. and Haschemeyer,A.E. (1976) Liver protein synthesis. Molecular weight distribution of pulse-labeled polypeptide chains in normal and thyroidectomized rats. *Biochim. Biophys. Acta*, **425**, 220–228.
12. Haschemeyer,A.E. (1969) Rates of polypeptide chain assembly in liver in vivo: relation to the mechanism of temperature acclimation in Opsanus tau. *Proc. Natl. Acad. Sci. U.S.A.* **62**, 128–135.
13. Yardeni,T., Eckhaus,M., Morris,H.D., Huizing,M. and Hoogstraten-Miller,S. (2011) Retro-orbital injections in mice. *Lab Anim. (NY)*, **40**, 155–160.
14. Martin,M. (2011) Cutadapt removes adapter sequences from high-throughput sequencing reads. *Embnet*, **17**, doi:10.14806/ej.17.1.200.
15. Kim,D., Pertea,G., Trapnell,C., Pimentel,H., Kelley,R. and Salzberg,S.L. (2013) TopHat2: accurate alignment of transcriptomes in the presence of insertions, deletions and gene fusions. *Genome Biol.*, **14**, R36.

16. Anders,S., Pyl,P.T. and Huber,W. (2015) HTSeq–a Python framework to work with high-throughput sequencing data. *Bioinformatics*, **31**, 166–169.

17. Ritchie,M.E., Phipson,B., Wu,D., Hu,Y., Law,C.W., Shi,W. and Smyth,G.K. (2015) limma powers differential expression analyses for RNA-sequencing and microarray studies. *Nucleic. Acids. Res.* **43**, e47.

18. Subramanian,A., Tamayo,P., Mootha,V.K., Mukherjee,S., Ebert,B.L., Gillette,M.A., Paulovich,A., Pomeroy,S.L., Golub,T.R., Lander,E.S. *et al.* (2005) Gene set enrichment analysis: a knowledge-based approach for interpreting genome-wide expression profiles. *Proc. Natl. Acad. Sci. U.S.A.*, **102**, 15545–15550.

19. Sakai,R., Winand,R., Verbeiren,T., Moere,A.V. and Aerts,J. (2014) dendsort: modular leaf ordering methods for dendrogram representations in R. *F1000Res*, **3**, 177.

20. Schneider-Poetsch,T., Ju,J., Eyler,D.E., Dang,Y., Bhat,S., Merrick,W.C., Green,R., Shen,B. and Liu,J.O. (2010) Inhibition of eukaryotic translation elongation by cycloheximide and lactimidomycin. *Nat. Chem. Biol.*, **6**, 209–217.

21. Fresno,M., Jimenez,A. and Vazquez,D. (1977) Inhibition of translation in eukaryotic systems by harringtonine. *Eur. J. Biochem.*, **72**, 323–330.

22. Palmer,L.K., Shoemaker,J.L., Baptiste,B.A., Wolfe,D. and Keil,R.L. (2005) Inhibition of translation initiation by volatile anesthetics involves nutrient-sensitive GCN-independent and -dependent processes in yeast. *Mol. Biol. Cell*, **16**, 3727–3739.

23. Flaim,K.E., Jefferson,L.S., McGwire,J.B. and Rannels,D.E. (1983) Effect of halothane on synthesis and secretion of liver proteins. *Mol. Pharmacol.*, **24**, 277–281.

24. Bostrom,K., Wettesten,M., Borén,J., Bondjers,G., Wiklund,O. and Olofsson,S.O. (1986) Pulse-chase studies of the synthesis and intracellular transport of apolipoprotein B-100 in Hep G2 cells. *J. Biol. Chem.*, **261**, 13800–13806.

25. Merry,B.J. and Holehan,A.M. (1991) Effect of age and restricted feeding on polypeptide chain assembly kinetics in liver protein synthesis in vivo. *Mech. Ageing Dev.*, **58**, 139–150.

26. Braet,F. and Wisse,E. (2002) Structural and functional aspects of liver sinusoidal endothelial cell fenestrae: a review. *Comp. Hepatol.*, **1**, 1.

27. Lee,S., Liu,B., Lee,S., Huang,S.X., Shen,B. and Qian,S.B. (2012) Global mapping of translation initiation sites in mammalian cells at single-nucleotide resolution. *Proc. Natl. Acad. Sci. U.S.A.*, **109**, E2424–E2432.

28. Gao,X., Wan,J., Liu,B., Ma,M., Shen,B. and Qian,S.B. (2015) Quantitative profiling of initiating ribosomes in vivo. *Nat. Methods*, **12**, 147–153.

29. Zhang,P., He,D., Xu,Y., Hou,J., Pan,B.-.F., Wang,Y., Liu,T., Davis,C.M., Ehli,E.A., Tan,L. *et al.* (2017) Genome-wide identification and differential analysis of translational initiation. *Nat. Commun.*, **8**, 1749.

30. Archer,S.K., Shirokikh,N.E., Beilharz,T.H. and Preiss,T. (2016) Dynamics of ribosome scanning and recycling revealed by translation complex profiling. *Nature*, **535**, 570–574.

31. Gorochowski,T.E., Chelysheva,I., Eriksen,M., Nair,P., Pedersen,S. and Ignatova,Z. (2019) Absolute quantification of translational regulation and burden using combined sequencing approaches. *Mol. Syst. Biol.*, **15**, e8719.

32. Ward,W. and Richardson,A. (1991) Effect of age on liver protein synthesis and degradation. *Hepatology*, **14**, 935–948.

33. Rattan,S.I. (1996) Synthesis, modifications, and turnover of proteins during aging. *Exp. Gerontol.*, **31**, 33–47.

34. Zou,K., Ouyang,Q., Li,H. and Zheng,J. (2017) A global characterization of the translational and transcriptional programs induced by methionine restriction through ribosome profiling and RNA-seq. *BMC Genomics*, **18**, 189.

35. Kaeberlein,M. and Kennedy,B.K. (2011) Hot topics in aging research: protein translation and TOR signaling, 2010. *Aging Cell*, **10**, 185–190.

36. Anisimova,A.S., Meerson,M.B., Gerashchenko,M.V., Kulakovskiy,I.V., Dmitriev,S.E. and Gladyshev,V.N. (2020) Multifaceted deregulation of gene expression and protein synthesis with age. *Proc. Natl. Acad. Sci. U.S.A.*, **117**, 15581–15590.

37. Conn,C.S. and Qian,S.B. (2013) Nutrient signaling in protein homeostasis: an increase in quantity at the expense of quality. *Sci. Signal*, **6**, ra24.

38. Morimoto,R.I. and Cuervo,A.M. (2014) Proteostasis and the aging proteome in health and disease. *J. Gerontol. A Biol. Sci. Med. Sci.*, **69**(Suppl. 1), S33–S38.

39. Truitt,M.L. and Ruggero,D. (2016) New frontiers in translational control of the cancer genome. *Nat. Rev. Cancer*, **16**, 288–304.

40. Armistead,J. and Triggs-Raine,B. (2014) Diverse diseases from a ubiquitous process: the ribosomopathy paradox. *FEBS Lett.*, **588**, 1491–1500.